Title
Global Optimization of Adsorbate Covered Supported Cluster Catalysts: The Case of $Pt_7H_{10}CH_3$ on α-Al_2O_3

Journal
ChemCatChem, 12(3)

ISSN
1867-3880

Authors
Zhai, Huanchen
Sautet, Philippe
Alexandrova, Anastassia N

Publication Date
2020-02-06

DOI
10.1002/cctc.201901830

Global Optimization of Adsorbate Covered Supported Cluster Catalysts: the Case of $Pt_7H_{10}CH_3$ on α-Al_2O_3

Huanchen Zhai,[1] Prof. Dr. Philippe Sautet[1,2,*], and Prof. Dr. Anastassia N. Alexandrova[1,3,*]
[1]*Department of Chemistry and Biochemistry, University of California, Los Angeles, 607 Charles E. Young Drive East, Los Angeles, California 90095, United States*
[2]*Department of Chemical and Biomolecular Engineering, 5513 Boelter Hall, University of California, Los Angeles, Los Angeles, California 90095, United States*
[3]*California NanoSystems Institute, 570 Westwood Plaza Building 114, Los Angeles, California 90095, United States*

*Corresponding Authors: E-mail: ana@chem.ucla.edu, sautet@ucla.edu

Abstract

Determining structures of supported sub-nanometer catalytic clusters is important for finding binding sites, active sites, and reaction mechanisms. In realistic conditions, the cluster may be covered with adsorbed reactants and intermediates, which strongly affect the structure of the cluster compared to the low coverage regime. The global optimization of supported adsorbate-covered clusters is not possible with existing methods. We present a customized Basin Hopping (BH) approach, with a core (metal cluster) – shell (adsorbates) separation scheme, and perform first applications to the search of low-energy isomers of Pt_7/α-Al_2O_3 at high hydrogen coverage (10H). The presence of adsorbates significantly alters the low-energy isomers compared to bare Pt_7/α-Al_2O_3. Molecular dynamics simulations additionally show the different time-scales associated with the mobility of H and Pt atoms. The revised BH method with core-shell separation presents key advantages for the structural exploration of adsorbate-covered supported catalysts, relevant to realistic catalytic conditions.

Introduction

Oxide surface supported catalytic sub-nanometer platinum clusters have found wide application in industrial reactions involving (de-)hydrogenation of hydrocarbons, such as naphtha reforming and alkane non-oxidative dehydrogenation [1-7] Industrial catalysts correspond to low loading of Pt supported on alumina, with a corresponding particle size of 0.6 to 1.1 nm. [8] However, the detailed catalytic mechanism of these reactions has not been fully elucidated despite the efforts expended over the years, which is partly due to the difficulty in characterizing the shape, size and active sites of the cluster in this "non-scalable" regime. The problem becomes even more complicated when considering realistic conditions, including high hydrogen coverage and finite temperature effects. [9,10]

Global optimization is the standard procedure for exploring Potential Energy Surface (PES) and identifying the most stable structure of catalytic clusters. [11-13] For gas phase and surface supported clusters, many different global optimization approaches have been extensively studied, including genetic algorithm, [14,15] Basin Hopping (BH), [16,17] and neural network fitting.[13,18,19] After the shape of catalytic clusters is identified by global optimization, the global minimum structure and possibly some other low-energy isomers can be selected as reference states, for studying active sites for various reactants and corresponding reaction pathways. [7, 20-22] However, despite the relatively low computational cost, this scheme may not be reliable if the low-energy bare-cluster isomers do not appear to be the most active ones, or if a big shape change occurs upon the adsorption of reactants. In particular, this will be the case when the catalytic cluster itself is highly fluxional, or if adsorbates affect the cluster shape. [23, 24] In this situation, the actual geometry change can only be tracked through a global optimization for the whole system, including the cluster, reactants and hydrogen coverage. This is a highly challenging task as the configuration space is significantly larger than that for a routine global optimization. It also requires adapted algorithms to preserve the identity of the reactant adsorbate during global optimization.

In 2011, an early computational study by Sautet and coworkers presents a surface stability diagram for a Pt_{13} cluster supported on γ-Al_2O_3 indicating the H coverage as a function of H_2 pressure and temperature. It shows that a high H coverage can be reached and that the cluster structure changes from biplanar to cuboctahedral geometry when high hydrogen coverage is above 18 H atoms per 13 Pt atoms, [23] where molecular dynamics (MD) simulations have been used to obtain the low-energy isomer of hydrogen adsorbed structure. It was followed in 2013 by a study of the C_1 and C_2 intermediates resulting from the dissociative adsorption of ethane on the supported Pt cluster, showing a strong influence of the nature of the intermediate on the equilibrium H coverage and on the cluster shape. [25] Very recently, using the similar MD approach Chizallet et al studied PtSn clusters supported on γ-Al_2O_3, at different hydrogen coverage. The study shows that both Pt/Sn ratio and number of hydrogens play an important role in cluster shape and properties. [24] In 2015, a computational study performed by Pacchioni et al indicates that, at high hydrogen coverage, hydrogen atoms can transfer from Ru_{10} cluster to surface, where the support are anatase TiO_2 and tetragonal ZrO_2 (101) surfaces, but the complete global optimization was not used in the study. [26] Recently, Sun and Sautet proposed a modified genetic algorithm for global optimization of gas phase

Pt_{13} cluster with high hydrogen coverage, which shows the importance of considering low-energy metastable cluster isomers in reactions. [27]

We present a method for global optimization of surface-supported Pt clusters under high hydrogen coverage, based on a modified BH scheme. The $Pt_7H_{10}CH_3$ on α-Al_2O_3 will serve as a testing system, as the bare-cluster version of this system has been intensively studied in our previous work. [28] The Pt_7 size is both realistic for a subnanometer size cluster and its global optimization with 11 adsorbates is computationally feasible. An initial coverage of 9 H is selected, since this corresponds to 1.3 H per Pt, a realistic coverage at typical temperature (800 K) and H_2 pressure (1-10 bar) used in catalytic reforming reactions. [4] It should be noted that such small Pt cluster show a H coverage about 3 times higher than larger particles so that the chosen number of H atoms is hence far from the saturation coverage (~ 21 H).[29] Methane is used as a model alkane and a first intermediate for its dehydrogenation ($H+CH_3$) is added to the hydrogenated cluster, hence providing the $Pt_7H_{10}CH_3$ formula. In our approach for the global optimization of adsorbate covered supported cluster, we first improved the initial structure generation algorithm based on bond length distribution by introducing constraints on the bonding element types. Then the core-shell separation is used in the perturbation step in BH method, to help keeping the integrity and reasonableness of the perturbed structure. MD simulation is also utilized in our approach to examine the relative mobility of the atoms in the core and shell parts, justifying the core-shell separation. We found that the presence of high coverage with H has a significant influence on Pt_7 geometry and fluxionality, which indicates that a global optimization of the whole system is indeed necessary.

Methods

1. Initial structure generation

The method of initial structure generation for starting BH global optimization is based on Bond Length Distribution Algorithm (BLDA) proposed in our previous work, [13] which has been successfully applied to adsorbate-free Pt_7 supported on α-alumina. [28] In BLDA, the structure is constructed by each time adding one atom or fragment to the existing structure. The position of new atom is determined by selecting the distance between the new atom and one old atom from a normal distribution. In this work, in order to create the cluster structure with hydrogen coverage, we first add Pt atoms (core part), then add CH_3 and H atoms (shell part) (Figure 1), because it is known that these adsorbates bind on the surface of Pt clusters and do not migrate inside the small Pt cluster. To further improve the initial guess, in this case, the ways Pt atoms and adsorbates are added are slightly different. The new Pt atom is required to be connected to at least two atoms already in the system (including existing Pt atoms and surface atoms), while the new CH_3 fragment or H atom is required to be connected to at least one Pt atom in the cluster. Thus the H atoms can take both atop and bridge sites, or somewhere in-between.

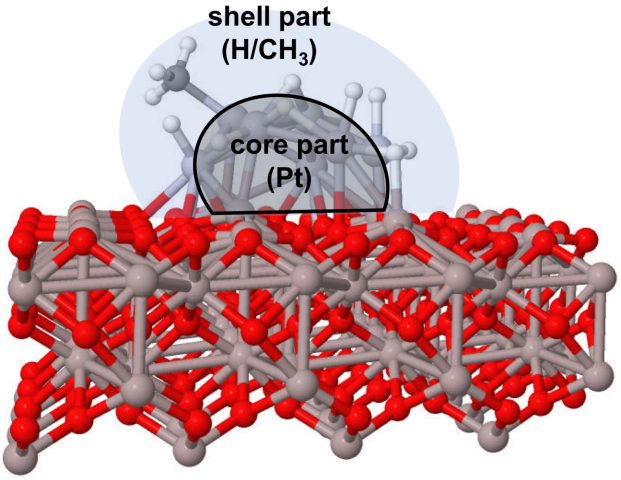

Figure 1. Core-shell separation of $Pt_7H_{10}CH_3$ structure supported on the α-Al_2O_3 (0001) surface slab model.

2. Basin hopping global optimization

The traditional BH global optimization is based on a canonical Monte Carlo (MC) simulation, [16] where at each step the coordinates of the current structure are perturbed by a random distance (called perturbation), and the resultant structure is then geometrically optimized to a local minimum. The optimized structure can be either discarded or accepted, and the decision is based on the probability dependent on energy difference from previous accepted structure and the temperature. Several issues arise when this approach is applied to a surface supported cluster under high coverage. Taking our testing system as an example, first of all, the perturbed $Pt_7H_{10}CH_3$ structure can easily become disconnected, if the default perturbation distance for Pt is of the same order of magnitude as the Pt-H bond length. Secondly, the CH_3 fragment may lose integrity during the random perturbation. We also note that the α-Al_2O_3 surface atoms are not very mobile during the optimization. It is thus reasonable to not move any oxide surface atoms during the perturbation. However, the perturbed Pt atoms may then be at a too short distance from the surface atoms, which would possibly introduce some difficulties in the Self-Consistent Field (SCF) procedure in Density Functional Theory (DFT) calculation.

We have introduced a partial Force Field (FF) optimization to solve the short-distance problem, which is applied after the perturbation. A Lennard-Jones (LJ) potential is used to represent the FF, where the equilibrium separation is selected to be the sum of covalent radii of the pair of elements. The FF optimization is partial in the sense that it will terminate after no pair of atoms has a distance smaller than 0.7 times the sum of covalent radii, which means that this partial optimization will not lead the structure to a local minimum on the FF PES, but will only make it good enough for starting a DFT optimization. At very short pair-distance, the force of the system is dominated by the pairwise nuclear repulsion, which is classical and can be reasonably approximated by the LJ potential.

Similar to some other BH implementations, we introduced the site swap operation (with a 25% occurrence rate) for CH_3 fragment, before the actual perturbation. During this operation, the CH_3 fragment is randomly swapped with a hydrogen atom, in order to moderately sample all possible CH_3 binding sites. In addition, in order to keep the core-shell structure of the system, we perform the

perturbation of atoms in core part and shell part separately. As a first step, each H/CH_3 is labeled by the index of cluster atom to which it is bound. Then all cluster atoms are randomly perturbed, with a magnitude of distance equal to 0.4 times the covalent radius of the elements (Pt, in our case). Then the cluster and surface part are partially optimized using FF to make sure that no two cluster atoms are too close to each other (with the surface part kept fixed). After this, H/CH_3 are moved by exactly the same distance and direction as the cluster atom they bind to. In the Pt cluster case, this process guarantees that the Pt-H and Pt-C bonds are unchanged after the perturbation of Pt atoms. Then we apply the perturbation on H/CH_3 coordinates, with a magnitude of distance equal to 0.6 times the covalent radius of the elements (H or C). Here, the factor for the perturbation distance is larger for light elements, since light element atoms are in general more mobile than heavy cluster atoms. The partial FF optimization is then applied again, this time for the whole system (with cluster and surface part kept fixed). Finally, we need to detect whether the structure becomes disconnected after the perturbation. If any atom or fragment is separated from the main structure, it will be added back using the initial structure generation algorithm discussed above. Details of the implementation of the algorithm is provided in Supporting Information.

3. Binding site sampling

Due to the large number of atoms in the system under consideration ($Pt_7H_{10}CH_3$) and high mobility of hydrogen atoms compared with the cluster core, or pure Pt cluster systems, we note that in practice the above BH process may actually miss the true global minimum or some important low-energy local minima, if only thousands of structures are optimized and sampled. Instead, it is much easier for the BH to find the low-energy core part (whose composition is Pt_7 in our test system). Upon the optimized core part, the H/CH_3 adsorbates can occupy different binding sites, producing a large number of configurations. Therefore, it would be possible to get a better candidate global minimum, by keeping some of the found Pt core parts found by BH, and sampling more binding sites for H/CH_3.

In our work, a random binding site sampling is performed for several low-energy isomers obtained from BH optimization. For each isomer, we randomly change the binding site of the CH_3 fragment, and/or several H atoms, to generate new structures. These new structures are then optimized to nearest local minima to see if they can give new lower-energy isomers.

4. Density Functional Theory calculation

The DFT calculation is performed using Vienna Ab initio Simulation Package (VASP) 5.4.4, [30] with the Projector Augmented-Wave (PAW) method [31] and the Perdew-Burke-Ernzerhof (PBE) functional. [32] The 4 × 4 slab model for α-Al_2O_3 (0001), with lattice constants a = 4.807 Å and c = 13.117 Å. After adding cluster part, the vacuum gap along direction normal to the surface is at least 15 Å. To reduce the computational cost, the thickness of slab model is $c/2$, with lower half kept fixed during geometry optimization, and only Γ point is sampled in k-space. dDSC vdw correction [33,34] is used in the geometry relaxation step of the global optimization. The kenergy cutoff is set to be 500 eV for final results.

Result and Discussion

The global optimization of $Pt_7H_{10}CH_3$ deposited on α-Al_2O_3 surface was performed by 10 parallel BH walkers, with each walker moving 300 steps. After the BH optimization, more than 1,800 additional geometry optimization were performed for binding site sampling. In total, 1,124 geometrically unique local minima were found for the system, spanning an energy range of 3.0 eV. The energy distribution of all found local minima is shown in Figure 2(a). There are 58 local minima in the low-energy range (up to 0.4 eV above the energy of putative global minimum (GM)). In our previous study, we found that, for the bare Pt_7 cluster deposited on α-Al_2O_3, there are only 11 unique local minima within the 0.4 eV energy range. The reason for the increase in number of low-energy isomers appears to be the geometric variety of the adsorbed H/CH_3. In fact, many of the $Pt_7H_{10}CH_3$ structures share the same Pt_7 core shape. The 58 local minima can be classified into 6 categories (labeled by A, B, C, D, E and F), according to their Pt_7 core geometries, as shown in Figures 2(b) and 3. Table 1 lists the number of structures in each core shape category. We can see that none of these core shapes dominates the low-energy region.

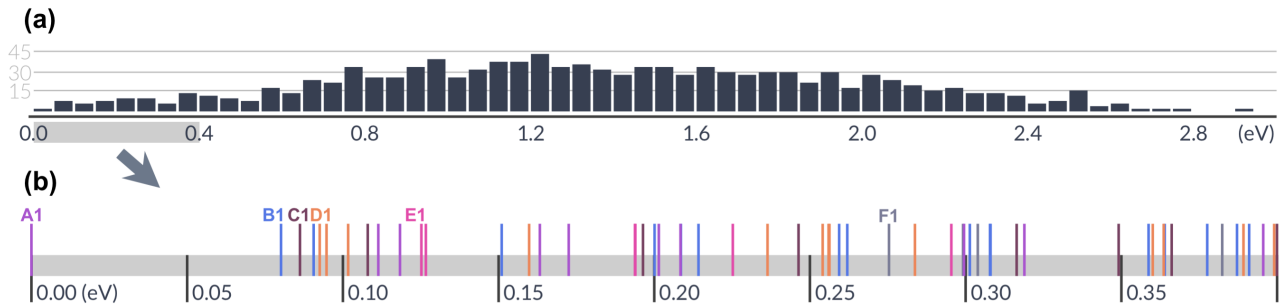

Figure 2. (a) Energy distribution of geometrically unique local minima of $Pt_7H_{10}CH_3$ clusters with respect to the putative global minimum, found by global optimization (the number of isomers within the given energy window in the histogram is shown on the ordinate). The shaded gray area is expanded in part (b). (b) Energy spectrum of low-energy isomers within the energy range of 0 to 0.4 eV with respect to the energy of the putative global minimum (isomer A1). Different colors and letters (A to F) correspond to different Pt_7 core structures (see Figure 3).

Table 1. Number of different isomer structures for each Pt_7 core shape within the energy range of 0 to 0.4 eV with respect to the energy of the putative GM (isomer A1).

Pt_7 core shape	A	B	C	D	E	F
Number of structures	10	16	9	13	6	4

Figure 3 shows the lowest-energy structures in each Pt_7 core categories. It is worth noting that the Pt_7 core structures in $Pt_7H_{10}CH_3$ have very low similarity to those of bare Pt_7, which implies that the adsorption of H/CH_3 has a significant influence on the geometry of the Pt_7 cluster. In particular, Structures B1, C1 and D1 have a singled out Pt atom, coordinating with only one other Pt atom.

However, this kind of structure is not stable in the absence of adsorbates (does not appear in low-energy region). Obviously, the change of geometry has to be related to the number of H atoms adsorbed, since less compact Pt_7 core structure should allow better Pt-H interactions. The low similarity in bare and adsorbed Pt_7 clusters indicates that taking bare Pt_7 structure as reference states to help exploring PES of adsorbed clusters is incorrect, as it misses some important local minima and core shapes.

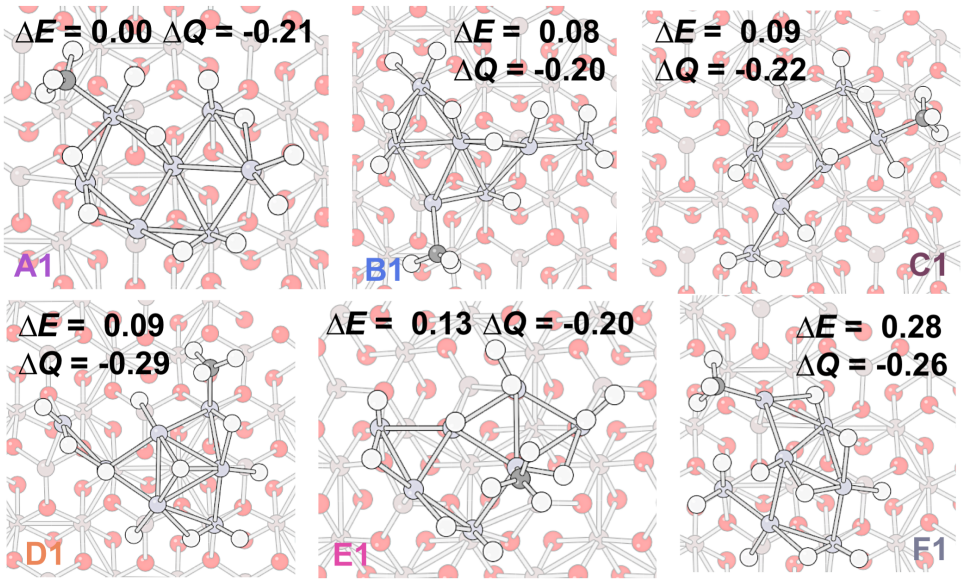

Figure 3. Isomer structures of each Pt_7 core shape (A to F) with lowest-energy for the alumina-supported $Pt_7H_{10}CH_3$ cluster found by global optimization. Energy (ΔE, in eV) is relative to the energy of putative GM (isomer A1). Charge (ΔQ) is the sum of Bader charge in the atoms of the cluster part ($Pt_7H_{10}CH_3$).

Figure 4 shows the occurrence probability of all core shapes at different temperature, based on electronic energies (vibrational entropy contribution to the probability has been ignored, as an approximation), and Boltzmann statistics. Constructing such "hot" phase diagrams for catalytic systems, in order to elucidate the structures that emerge within the state of the catalyst at temperatures of interest and remove the focus on the GM alone, has been introduced by Zhang, Hermans, and Alexandrova. [35] It is necessary because often, higher energy structures in the ensemble are responsible for the catalysis. [6,7,10,27,36-37] Since many structures are close in energy in the studied case, many of them would be populated and constitute the state of the catalytic system at finite temperatures. Below 200 K, the ensemble primarily consists of the structures of type A, with negligible contributions from other structures. As the temperature increases the probabilities of other core types increases. In particular, in the window of 700-900 K, typical for Pt-catalyzed dehydrogenation reactions, isomers of the types A-E contribute on the nearly equal footing. In each type of Pt core structure, several isomers are present due to different positions of H atoms. Any or all of these isomers could be relevant for the catalytic mechanism.

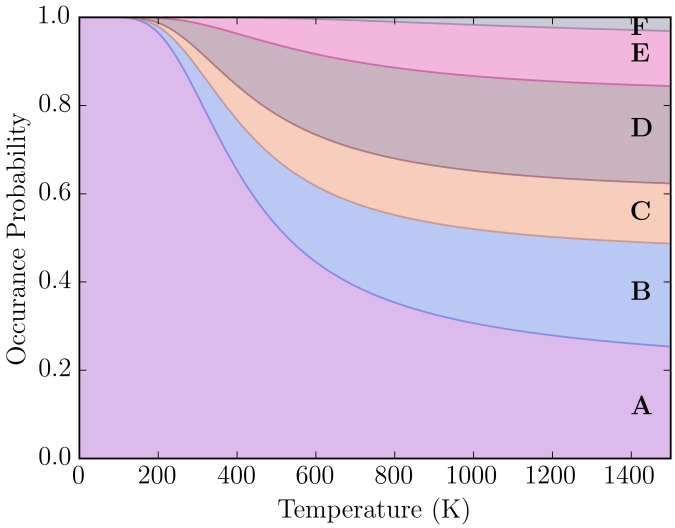

Figure 4. Occurrence probability of Pt_7 core shapes (A to F) for $Pt_7H_{10}CH_3$ on alumina at different temperature, based on Boltzmann distribution of electronic energies.

Since the Pt_7 core shapes are A and B are among the dominant, and also have slightly larger number of accessible local minima, we focus on these two categories for the analysis of H binding sites. Figures 5 and 6 show the geometries and charges of some of the low-energy isomers belonging to the Pt_7 shapes A and B. In every structure, H atoms occupy bridge and atop sites, while CH_3 is always on an atop site (with one exception being B3). In some structures, such as the putative GM A1, and B4, there are several H atoms binding to the CH_3 binding site, and this can be an initial structure for the recombination and desorption of CH_4. On the other hand, in some other local minima, such as A5 and B1, there are no adjacent H atoms near CH_3. How these local minima can participate in CH_4 formation reaction, or inversely, be produced in the course of CH_4 binding and dissociation, is then related to the H atom mobility in this system, which will be covered in future part of this work.

Calculated Bader charges on atoms in the cluster are shown in Tables 2 and 3. In general, the charge transfer between the oxide surface and the cluster is small, with the cluster receiving ca. 0.2 electrons. In addition, the charge transfer between H/CH_3 adsorbates and Pt_7 is not significant, in most cases, indicative of covalent Pt-H and Pt-C bonding in the system, which is expected. One exception is the local minimum D1, where the summed charge on all ten H atoms is significant (-0.48). This is explained by one H atom taking the unique hollow site on the face of a 3-Pt triangle (as shown in Figure 3). The H atom in the hollow site has a charge of -0.19, which is very different from the charges of the H atoms occupying the atop or bridge sites.

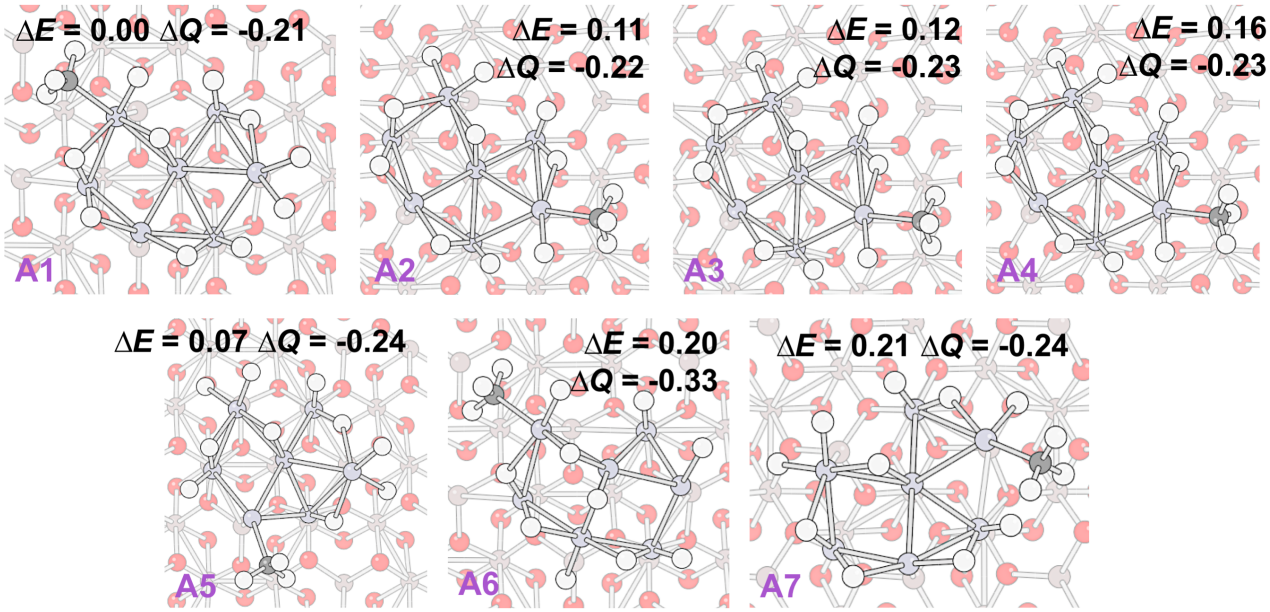

Figure 5. Low-energy structures of the Pt_7 core type A, of $Pt_7H_{10}CH_3$ clusters found by global optimization. Energy (ΔE, in eV) is relative to the energy of putative GM (isomer A1). Charge (ΔQ) is the sum of Bader charge in atoms of cluster part ($Pt_7H_{10}CH_3$).

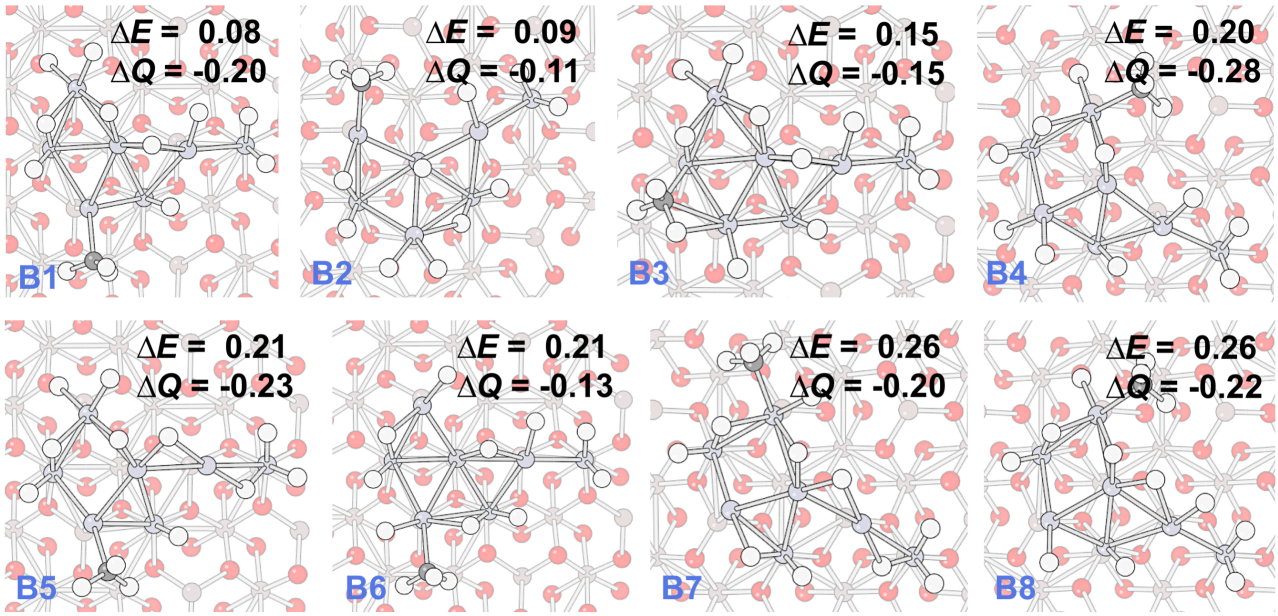

Figure 6. Low-energy structures of the Pt_7 core shape type B, of $Pt_7H_{10}CH_3$ clusters found by global optimization. Energy (ΔE, in eV) is relative to the energy of putative GM (isomer A1). Charge (ΔQ) is the sum of Bader charge in atoms of cluster part ($Pt_7H_{10}CH_3$).

Table 2. Bader charges on different parts of cluster for isomers of shape A-F with lowest energy. Charge Q(cluster) is the sum of the charge in all atoms of cluster part ($Pt_7H_{10}CH_3$).

isomer	$Q(CH_3)$	$Q(H_{10})$	$Q(Pt_7)$	Q(cluster)	isomer	$Q(CH_3)$	$Q(H_{10})$	$Q(Pt_7)$	Q(cluster)
A1	-0.08	-0.05	-0.09	-0.21	D1	-0.02	-0.48	+0.21	-0.29
B1	-0.06	-0.10	-0.05	-0.20	E1	-0.02	-0.25	+0.07	-0.20
C1	-0.07	-0.05	-0.10	-0.22	F1	-0.09	-0.17	0.00	-0.26

Table 3. Bader charges on different parts of cluster for some typical low-energy isomers of shape A and B. Charge Q(cluster) is the sum of the charge in all atoms of cluster part ($Pt_7H_{10}CH_3$).

isomer	$Q(CH_3)$	$Q(H_{10})$	$Q(Pt_7)$	Q(cluster)	isomer	$Q(CH_3)$	$Q(H_{10})$	$Q(Pt_7)$	Q(cluster)
A1	-0.08	-0.05	-0.09	-0.21	B1	-0.06	-0.10	-0.05	-0.20
A2	-0.03	-0.11	-0.08	-0.22	B2	-0.10	+0.20	-0.21	-0.11
A3	-0.03	-0.13	-0.07	-0.23	B3	-0.05	-0.08	-0.02	-0.15
A4	-0.04	-0.10	-0.09	-0.23	B4	-0.07	-0.12	-0.09	-0.28
A5	-0.07	+0.01	-0.18	-0.24	B5	-0.07	-0.11	-0.05	-0.23
A6	-0.09	-0.26	+0.02	-0.33	B6	-0.04	-0.01	-0.08	-0.13
A7	-0.10	0.00	-0.14	-0.24	B7	-0.07	-0.03	-0.10	-0.20
					B8	-0.07	-0.02	-0.13	-0.22

Born-Oppenheimer (DFT) MD simulations in the NVT ensemble at 700 K, have been performed on selected isomers to further study the fluxionality of the cluster structure. Note that, within the necessarily limited amount of sampling and lack of rare-event sampling techniques, MD is a method that would never recover the isomeric diversity clearly accessible to the system, as it would sample only a rather local configuration environment. MD is used in this work to qualitatively and visually assess the relative motilities of atoms in the system. Figures 7 and 8 are based on the MD trajectory starting from isomer A1, and Figures 9 and 10 are based on the MD trajectory starting from isomer B1. Each simulation lasted 10 ps, with the 1 fs time step. The first 1 ps of equilibration is not used for analysis.

We found that H atoms can be highly mobile at this temperature, while the Pt atoms are rather fixed at their positions. In both trajectories, some H atoms (circled in Figures 8 and 10) can change from bridge site to atop site, or the reverse. The *XY* position of H atoms along the trajectories (shown in Figure 7 and 9) spans a much larger area than that of Pt atoms, meaning that the H atoms are able to explore adjacent sites during this relative short simulation time.

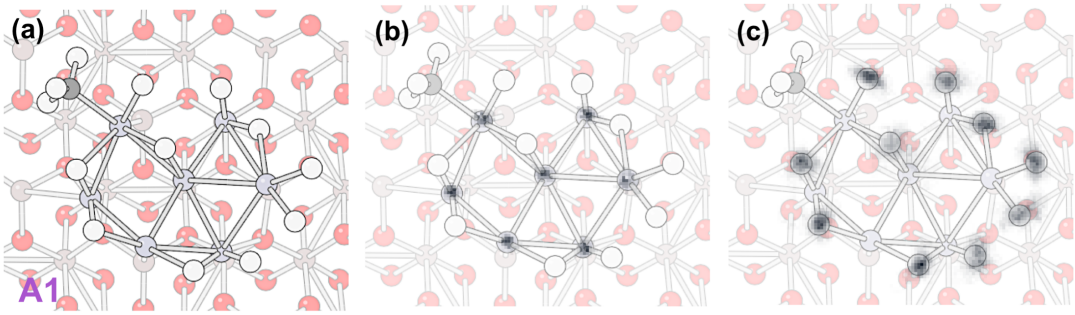

Figure 7. The probability of occurrence in *XY* plane of (b) Pt atoms and (c) adsorbed H atoms, during the MD trajectory starting from the isomer A1 (shown as a stationary structure in (a)). Darker color means higher probability for the atom taking certain *XY* position. Note that the darkness scales for (b) and (c) are different.

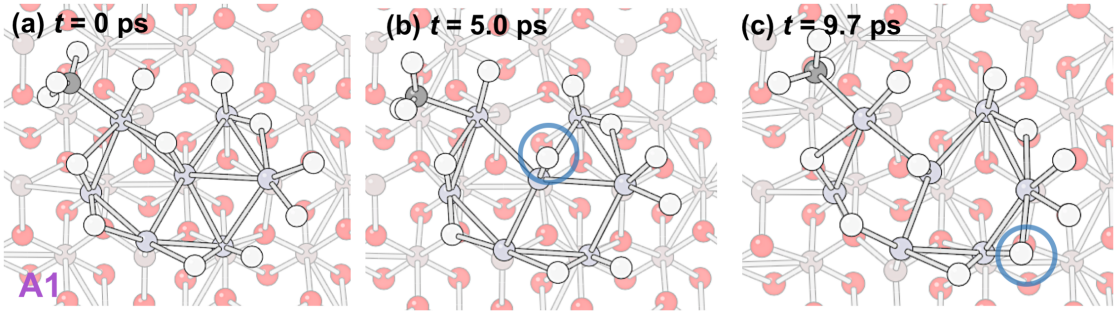

Figure 8. Cluster structure at simulation time *t* = (b) 5.0 ps and (c) 9.7 ps, during the MD trajectory starting from the isomer A1 (shown in (a)). The relocated H atoms are outlined.

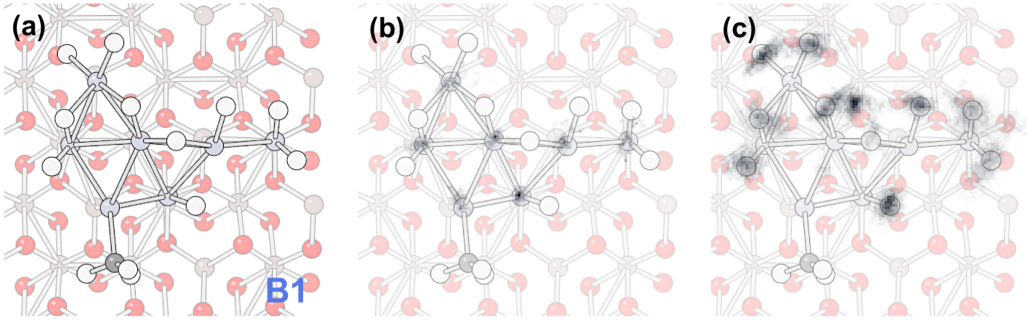

Figure 9. The probability of occurrence in *XY* plane of (b) Pt atoms and (c) adsorbed H atoms, during the MD trajectory starting from the isomer B1 (shown in (a)). Darker color means higher probability for the atom taking certain *XY* position. Note that the darkness scales for (b) and (c) are different.

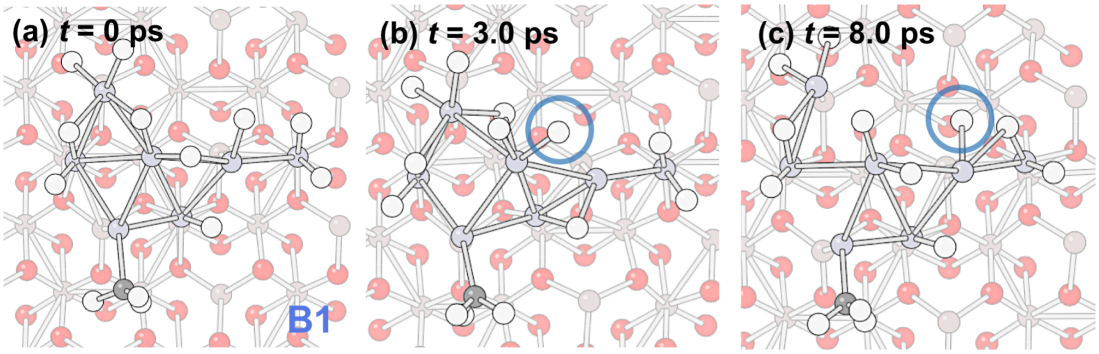

Figure 10. Cluster structure at simulation time t = (b) 3.0 ps and (c) 8.0 ps, during the MD trajectory starting from isomer B1 (shown in (a)). The relocated H atoms are outlined.

To further examine the mobility of H atoms, we calculated Mean Square Displacement (MSD) averaged over the Pt and H atoms (Figure 11). The MSD of the H atoms shows very different patterns for the trajectory starting from A1, comparing with that from B1, which is mainly due to the different PES property near isomers A1 and B1. As can be seen from Figure 7, for the trajectory starting from A1, the XY projections of different H atoms do not overlap. Therefore, the H atoms are mostly transiting between the bridge and the nearest atop sites, and do not interchange or shift any further. For the trajectory starting from B1, some irreversible change of the H binding site takes place. As a result, the structures shown in Figure 10 are quite different from each other. Hence, the MSD along the trajectory becomes very large at later simulation times. Nevertheless, in both cases we can see that the MSD averaged over all H atoms is significantly larger than that averaged over all Pt atoms. Therefore, we conclude that H atoms rearrange much more easily than Pt atoms in this system.

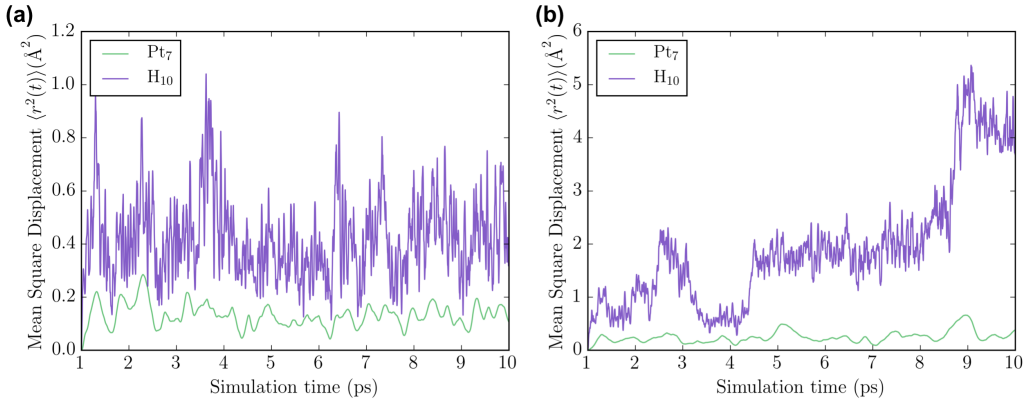

Figure 11. The MSD averaged over Pt (green) and H (purple) atoms, as a function of simulation time, calculated on MD trajectory at 700K starting from isomer (a) A1 and (b) B1.

Conclusions

In this work we propose a revised Basin Hopping global optimization approach, with core-shell separation, to address the challenging task of global optimization of surface-supported clusters with

high coverage of adsorbates. Using this revised method, we show that the high hydrogen coverage changes the preferred geometry of alumina-supported Pt_7 clusters. This observation implies that the isomers obtained from global optimization of the bare Pt_7 cluster on a support surface (or in the gas phase) may not be used as a "reference state" for the system with large number of adsorbates. For H-covered Pt_7 on α-Al_2O_3, a rich spectrum of isomers thermally-accessible at 700-900 K is found (700-900 K is a typical temperature range for catalytic dehydrogenation). Among the isomers, many have a common structure of the Pt core beneath the bound adsorbates, and thus these groups of isomers differ only by the adsorbate positions. Several typical core types, A-F, have been identified. Their presence in the statistical ensemble of the catalyst states changes as a function of temperature: The structures of the type A (which includes the global minimum) prevail below 200 K. Above that temperature, the contributions of the structures B-F grow, and at 700 K and above all of them become nearly equal with the population of A. Hence, all these states may play a role in a catalytic process on this cluster catalyst. In addition, for these H-covered systems, the H atoms and the Pt atoms have qualitatively different mobilities. This is seen not only from the appearance of the typical Pt core structures, A-F, but also from the ab initio MD simulations at 700 K, which show that Hs can quite easily move and change binding site on the cluster, while the Pt atoms are less mobile, and do not move in the time scale of the MD (10 ps). This further supports the idea that the general global optimization approach with a unified treatment for all atoms (those of the cluster and of the adsorbates) may not be very efficient for modelling catalytic clusters in realistic conditions, and further validates the method with the core-shell separation presented in this study.

Supporting Information

Implementation details of the perturbation step in BH algorithm, performance of BH algorithm, and coordinates of the 58 lowest-energy isomers (XYZ format) for $Pt_7H_{10}CH_3$.

Acknowledgments

This work was supported by DOE-BES Award DE-SC0019152. This research used resources of the National Energy Research Scientific Computing Center (NERSC), a U.S. Department of Energy (DOE) Office of Science User Facility operated under Contract No. DE-AC02-05CH11231, and the Argonne Leadership Computing Facility (ALCF) Facility, a DOE Office of Science User Facility supported under Contract DE-AC02-06CH11357, provided by the Innovative and Novel Computational Impact on Theory and Experiment (INCITE) program.

Keywords

Global optimization, heterogeneous catalysis, Pt clusters, fluxionality, dehydrogenation

References

1. J. H. Sinfelt, in *Handbook of Heterogeneous Catalysis*, (Eds.: G. Ertl, E. Knözinger, J. Weitkamp) Wiley, Weinheim, **1997**, pp. 1939–1955.

2. J.H.B. Sattler, J. Ruiz-Martinez, E. Santillan-Jimenez, B.M. Weckhuysen, *Chem. Rev.* **2014**, *114*, 10613.

3. Y. Barron, D. Cornet, G. Maire, F. G. Gault, *J. Catal*. **1963**, *2*, 152–155.

4. P. Raybaud, C. Chizallet, C. Mager-Maury, M. Digne, H. Toulhoat, P. Sautet, *J. Catal.* **2013**, *308*, 328–340.

5. M. D. Rötzer, A. S. Crampton, M. Krause, K. Thanner, F. F. Schweinberger, U. Heiz, *J. Phys. Chem. C* **2019**, *123*, 5518–5524.

6. E. Jimenez-Izal, B. C. Gates, A. N. Alexandrova, *Phys. Today* **2019**, *72*, 38–43.

7. E. T. Baxter, M.-A. Ha, A. C. Cass, A. N. Alexandrova, S. L. Anderson, S.L., *ACS Catal*. **2017**, *7*, 3322–3335.

8. A. Jahel, P. Avenier, S. Lacombe, J. Olivier-Fourcade, J. C. Jumas, *J. Catal*. **2010**, *272*, 275–286.

9. W. Zhao, C. Chizallet, P. Sautet, P. Raybaud, *J. Catal.* **2019**, *370*, 118–129.

10. H. Zhai, A. N. Alexandrova, *ACS Catal*. **2017**, 7, 1905–1911.

11. J. Zhang, M. Dolg, *Phys. Chem. Chem. Phys*. **2015**, *17*, 24173–24181.

12. J. Zhao, X. Huang, R. Shi, H. Liu, Y. Su, R. B. King, *Nanoscale* **2015**, *7*, 15086–15090.

13. H. Zhai, A. N. Alexandrova, *J. Chem. Theory Comput*. **2016**, *12*, 6213–6226.

14. A. N. Alexandrova, *J. Phys. Chem. A* **2010**, *114*, 12591–12599.

15. R. P. Kanters, K. J. Donald, *J. Chem. Theory Comput*. **2014**, *10*, 5729–5737.

16. D. J. Wales, J. P. Doye, *J. Phys. Chem. A* **1997**, *101*, 5111–5116.

17. Y. Zhao, X. Chen, J. Li, *Nano Res*. **2017**, *10*, 3407–3420.

18. X. Chen, M. S. Jørgensen, J. Li, B. Hammer, *J. Chem. Theory Comput*. **2018**, *14*, 3933–3942.

19. E. L. Kolsbjerg, A. A. Peterson, B. Hammer, *Phys. Rev. B* **2018**, *97*, 195424.

20. M. Gao, D. Horita, Y. Ono, A. Lyalin, S. Maeda, T. Taketsugu, *J. Phys. Chem. C* **2017**, *121*, 2661–2668.

21. D. H. Lim, J. Wilcox, *J. Phys. Chem. C* **2011**, *115*, 22742–22747.

22. J. C. Liu, Y. Tang, C. R. Chang, Y. G. Wang, J. Li, *ACS Catal*. **2016**, *6*, 2525–2535.

23. C. Mager-Maury, G. Bonnard, C. Chizallet, P. Sautet, P. Raybaud, *ChemCatChem* **2011**, *3*, 200–207.

24. A. Gorczyca, P. Raybaud, V. Moizan, Y. Joly, C. Chizallet, *ChemCatChem* **2019**, *11*, 1–12.

25. P. Raybaud, C. Chizallet, C. Mager-Maury, M. Digne, H. Toulhoat, P. Sautet, *J. Catal*.

2013, *308*, 328–340.

26. H. Y. T. Chen, S. Tosoni, G. Pacchioni, *ACS Catal*. **2015**, *5*, 5486–5495.
27. G. Sun, P. Sautet, *J. Am. Chem. Soc*. **2018**, *140*, 2812–2820.
28. H. Zhai, A. N. Alexandrova, *J. Phys. Chem. Lett*. **2018**, *9*, 1696–1702.
29. F. Behafarid, L. K. Ono, S. Mostafa, J. R. Croy, G. Shafai, S. Hong, T. S. Rahman, Simon R. Bare and B. Roldan Cuenya, *Phys. Chem. Chem. Phys*. **2012**, *14*, 11766-11779.
30. G. Kresse, J. Furthmüller, *Phys. Rev. B* **1996**, *54*, 11169.
31. P. E. Blöchl, *Phys. Rev. B* **1994**, *50*, 17953.
32. J. P. Perdew, K. Burke, M. Ernzerhof, *Phys. Rev. Lett*. **1996**, *77*, 3865.
33. S. N. Steinmann, C. Corminboeuf, *J. Chem. Phys*. **2011**, *134*, 044117.
34. S. Gautier, S. N. Steinmann, C. Michel, P. Fleurat-Lessard, P. Sautet, *Phys. Chem. Chem. Phys*. **2015**, *17*, 28921–28930.
35. Z. Zhang, E. Jimenez-Izal, I. Hermans, A. N. Alexandrova, *J. Phys. Chem. Lett*. **2019**, *10*, 20–25.
36. M.-A. Ha, E. T. Baxter, A. C. Cass, S. L. Anderson, A. N. Alexandrova, *J. Am. Chem. Soc*. **2017**, *139*, 11568–11575.
37. E. Jimenez-Izal, H. Zhai, J. Y. Liu, A. N. Alexandrova, *ACS Catal*. **2018**, *8*, 8346–8356.
38. E. Jimenez-Izal, J.-Y. Liu, A. N. Alexandrova, *J. Catal*. **2019**, *374*, 93–100.

TOC: A "core-shell" global optimization algorithm is proposed for surface-supported Pt clusters under the high coverage. A wide variety of thermally-accessible isomers of Pt_7 on alumina under hydrogen are identified, and many share the same Pt core, while feature the diverse placements and higher mobility of the adsorbates.